

# High-Throughput 3D Cell Invasion Chip Enables Accurate Cancer Metastatic Assays

Yuanqing Zhang<sup>†,‡</sup>, Ledu Zhou,<sup>\*,†,||</sup> and Lidong Qin<sup>\*,†,‡,§</sup>

<sup>†</sup>Department of Nanomedicine, Houston Methodist Research Institute, Houston, Texas 77030, United States

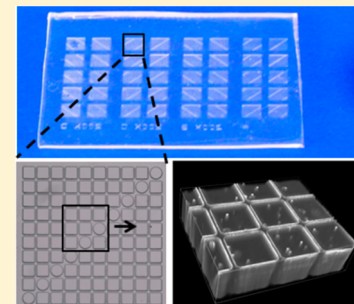
<sup>‡</sup>Department of Cell and Developmental Biology, Weill Medical College of Cornell University, New York, New York 10065, United States

<sup>§</sup>Department of Molecular and Cellular Oncology, The University of Texas M. D. Anderson Cancer Center, Houston, Texas 77030, United States

<sup>||</sup>Department of General Surgery, Xiangya Hospital, Central South University, Changsha, Hunan 410008, China

## Supporting Information

**ABSTRACT:** Chemotaxis is the phenomenon by which the migration and invasion of cells is directed in response to an extracellular chemical gradient. Chemotaxis of tumor cells and tumor-associated inflammatory and stromal cells is mediated by chemokines, chemokine receptors, growth factors, and growth factor receptors. Current techniques used to study chemotactic driven cell invasion and metastasis utilize two-dimensional migration assays involving imaging and analyzing tumor cells on glass slides or plastic surfaces, which requires large numbers of cells and often lacks real-time monitoring of vertical cell movement and systematically controlled chemotactic gradients, leading to contradictory results compared to those from clinical investigations and animal models. We addressed such challenges by developing a high-throughput microdevice with 4000 ultraminiaturized wells to monitor real-time, three-dimensional cell invasion over a wide range of cell densities and also screen drugs that inhibit cell invasion and potentially prevent metastatic malignancy. Additionally, this microdevice generates opposing gradients for two types of cells on the same chip, which builds a controlled system with sequentially changing components to study environmental effects from basal and immune cells.



## 1. INTRODUCTION

Tumor invasion and metastasis transform a primary tumor into a systemic and life-threatening disease.<sup>1</sup> The metastatic process involves a cascade of events, including cancer cell phenotypic transitions at the primary site,<sup>2</sup> tissue invasion,<sup>3</sup> circulation in blood or lymphatic systems,<sup>4</sup> and interaction with the cell microenvironment at the metastatic site<sup>5</sup> (Figure 1a). Tumor cell invasion is a complex, dynamic, and multistep process that has a crucial role in cancer metastasis. Local invasion begins with the activation of signaling pathways that control the distribution of certain proteins (e.g., actin) in cancer cells and the dissolving and softening of cell–matrix and cell–cell junctions, followed by enhanced cancer cell penetration into tissues, breaking of the basement membrane, and migration into neighboring tissue.<sup>6</sup> Recent studies have shown that cell invasion is also a social behavior related to the tumor microenvironment (i.e., presence of macrophages, fibroblasts, and other cells).<sup>7</sup> Clinical studies have sought to identify correlations between the number of tumor-associated macrophages (TAMs) and disease prognosis, and data have shown increased macrophage density or high TAM numbers are associated with poor prognosis.<sup>8</sup> For example, TAMs were shown to promote breast carcinoma cell invasion, but the complete molecular mechanism of cell invasion and metastasis is still unclear. Researchers rely on *in vitro* invasion assays to

characterize metastatic capability, and an effective assay to quantify invasive capacity is required to more accurately study and diagnose cell invasiveness.

Traditional laboratory techniques used to study cell invasion and metastasis utilize imaging and analyzing tumor cell migration on glass slides or flat, two-dimensional (2D) plastic surfaces.<sup>9</sup> These 2D substrates provide little quantitative information about cell–matrix interactions, tumor invasion, or cell–cell interactions during migration and invasion.<sup>10</sup> Recent studies have shown that 2D systems cannot provide a complete picture of three-dimensional (3D) tumor cell adhesion and invasion.<sup>11</sup> For example, because cancer cells infiltrate a stromal environment dominated by cross-linked networks of type I collagen, the role of antimatrix metalloproteinase (MMP) molecules in mediating migration (which is intrinsically associated with the mechanical and structural properties of the matrix)<sup>10</sup> cannot be fully captured in 2D environments. A low-cost, high-throughput, and real-time 3D cell invasion assay is needed to accurately study tumor invasion and metastasis.<sup>12</sup> The ideal assay would enable easy manipulation, quantification by digital analysis and morphological study, downstream biochemical assays, and close recapitulation of the *in vivo*

Received: July 23, 2014

Published: October 6, 2014

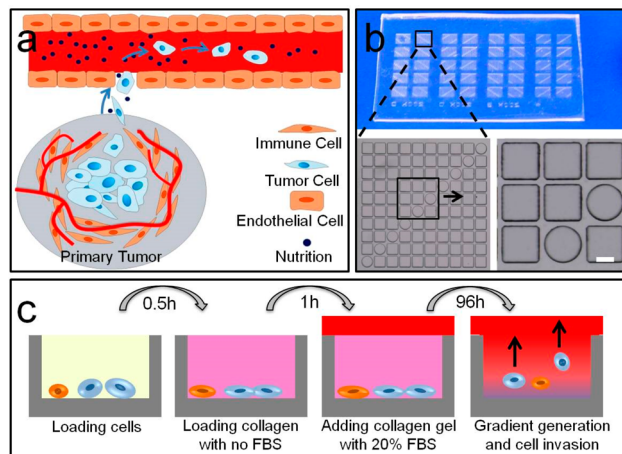


**Figure 1.** Design and operation of the MI-Chip device for 3D cell invasion studies. (a) Schematic of the process of invasion of metastatic cells into blood vessels. (b) Chip design and dimensions: 4000 ultraminiaturized microwells consist of four like-numbered components; each component contains 10 sets of  $10 \times 10$  microwells. Scale bar:  $100 \mu\text{m}$ . (c) Schematic of device operation.

setting.<sup>3</sup> Microfabrication-assisted technology using microscale arrays of round or rectangular wells, channels, or other simple patterns has the potential to address these issues.<sup>13</sup>

Here, we present a high-throughput 3D cell invasion assay using 4000 ultraminiaturized wells to monitor cell invasion in real-time (Multiwell Invasion Chip: MI-Chip; Figure 1b). In this system, cells are randomly placed or arranged within a gradient at the bottom of microwells filled with collagen gel, and nutrients are placed on top of the collagen layer. Cells are then allowed to gravitate from the collagen gel toward the nutrition layer, and images are captured at sequential focal planes in the gel at preset time points. The invasive capacity of either a single cancer cell or cells at various densities can be evaluated. The capabilities of the MI-Chip could be extended to generate opposing gradients comprised of two different cell types on the same chip, which could be used to study the correlation between macrophage numbers and cancer cell invasiveness. By applying various antimetastatic drugs to the 3D migration assay, we can easily adapt the MI-Chip to efficiently screen potential invasiveness inhibitors. The MI-Chip can perform thousands of experiments with one run and provide not only accurate and comprehensive information on cell invasiveness but also selection of candidate drugs to inhibit malignancy.

## 2. RESULTS

**2.1. Fabrication and Operation of the MI-Chip.** The MI-Chip was fabricated with poly(dimethylsiloxane) using a photolithographic process as summarized in the Figure S1 and described previously.<sup>14</sup> The MI-Chip consists of 4000 ultraminiaturized wells distributed in four compartments, each compartment containing 10 arrays of  $10 \times 10$  microwells. These  $10 \times 10$  microwells are produced in two shapes, square with a bottom size of  $200 \times 200 \mu\text{m}^2$  or round with a  $200 \mu\text{m}$  diameter and are arranged in sequential patterns for mapping and identification,<sup>15</sup> (Figures 1b and S2). In a subsequent cell invasion study, we only calculated the cells loaded in the square shape microwells. The depth of all microwells is approximately  $160 \mu\text{m}$  (Figure S3), which can be further enlarged to meet 3D requirement by changing the fabrication procedure. *In vivo*,

directional movement of cancer cells develops at distances typically  $100\text{--}150 \mu\text{m}$  beyond the diffusion capacity of chemokines and oxygen from blood vessels or in areas of a tumor with compromised blood flow due to aberrant vasculature formation.<sup>16</sup> The depth of  $160 \mu\text{m}$  is able to mimic real 3D invasion by providing sufficient spacing for chemotaxis.

We first treated the surface of the microwells with basement membrane extract (BME) solution to facilitate cell adhesion.<sup>17</sup> Cells were then loaded into the microwells randomly or using a gradient and BME was replaced with  $2 \text{ mg/mL}$  serum-free collagen gel. Next,  $8 \text{ mg/mL}$  collagen gel containing  $20\%$  fetal bovine serum (FBS) was carefully placed across all the microwells as a barrier to generate a chemoattractant gradient after nutrient addition on top (Figure 1C) that can be stably maintained within  $160\text{--}200 \mu\text{m}$  during the experiment (Figure S4). Random cell deposition can be accomplished by spreading cells with a pipet. Three hundred microliters of cell suspension are dispensed onto the chip and spread over the chip area, and the cells are randomly settled into the microwells by gravity. A single cell assay can be performed using a suspension of cells diluted in culture medium to  $5 \times 10^4 \text{ cells/mL}$ ; at this dilution, approximately  $34\%$  of the wells will contain single cells. Increasing cell concentrations resulted in an additional  $50$  single cells in individual wells (Figure S5). Gradient cell seeding was generated by inserting the chip into a homogeneous suspension of cells at a preset angle.<sup>18</sup> Cell numbers ranged from  $0$  to  $50$  cells along the tilted chip automatically formed by the sedimentation of cells in the wells with a tilt angle of  $45^\circ$  and a concentration of  $10^6 \text{ cells/mL}$  (Figure 2).

**2.2. Single-Cell Invasion Assay.** We first studied the invasive behaviors of breast cancer cells on the MI-Chip. We utilized two different breast cancer cell lines in our study, the highly metastatic SUM-159 cell line and the tumorigenic but nonmetastatic MCF-7 cell line. Both cell types were transfected with the gene for green fluorescent protein (GFP) to allow 3D

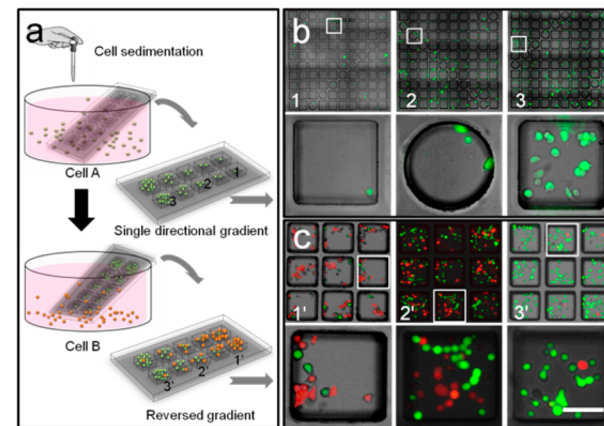


**Figure 2.** Generation of cell density gradients. (a) Steps of the experimental setup. The MI-Chip was placed at a specific tilt angle in a beaker filled with a homogeneous suspension of cells. Because of the varying volume of cells available for sedimentation above the chip, cells are deposited into the microwells with a density gradient. (b) Fluorescence micrographs showing cell density gradients generated on the MI-Chip. (c) Fluorescence micrographs showing the generation of reverse gradients in cell densities for SUM-159/GFP cells (green) and macrophages (red) on the same MI-Chip after two consecutive sedimentation processes in opposite directions. The white box was selected magnified area. Scale bar:  $100 \mu\text{m}$ .

fluorescent imaging of the cells as they penetrated into the collagen. Real-time tracking of cell movement allowed us to characterize metastatic invasion under controlled spatiotemporal conditions. By adjusting the focal plane of the microscope, bright-field and fluorescent images ( $20\times$ ) of cells on the top layer of the microwells could be recorded each day (Figure 3a–

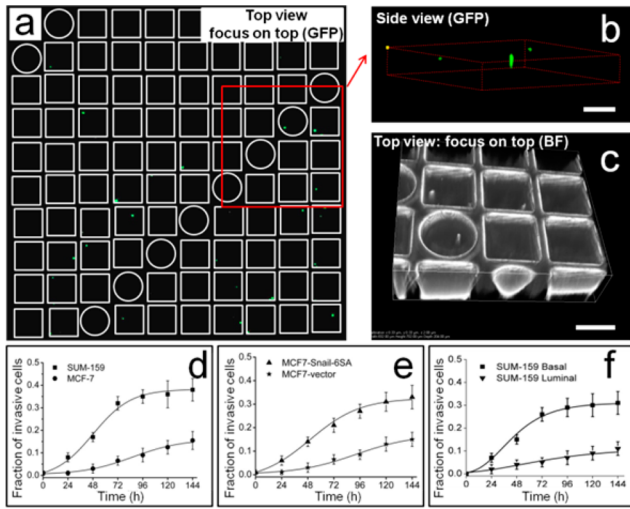


**Figure 3.** Single cancer cell invasion assay. (a) GFP image of invasive cells on the top layer of the microwells. The focal plane of the fluorescent microscope was adjusted to image cells located on the top layer of the microwells. (b) The image of a partial MI-Chip using a confocal microscope shows the cells located on the top layer of the microwells. Scale bar:  $200\ \mu\text{m}$ . (c) 3D image of invasive cells on the top layer of the microwells. A z-stack of bright-field (BF) images has been acquired with a step size of  $1\ \mu\text{m}$  using a wide-field microscope. The stack of images is reconstructed using the software provided by the microscope manufacturer. Scale bar:  $200\ \mu\text{m}$ . (d–f) Invasion capacity of a single cell derived from MCF-7 and SUM-159. Comparison of fractions of invasive cells for MCF-7 and SUM-159 cells (d); MCF-7 vector and MCF-7 Snail-6SA cells (e); and SUM-159 basal-like ( $\text{CD}44^+\text{CD}24^-$ ) and luminal-like ( $\text{CD}24^+\text{CD}44^-$ ) cells (f).

c). Time-lapse images of the cell invasion process were captured, and the fraction of invasive cells was plotted. In the absence of a chemoattractant, few SUM-159 cells moved toward the top layer; instead, the cells appeared to move randomly along the bottom of the microwells (Figure S6). Conversely, after loading 20% FBS collagen gel on the top layer of the microwells as a chemoattractant, we observed chemotactic movement of SUM-159 cells toward the FBS-containing gel (Figure 3d). Thus, the metastatic cell line penetrated a collagen matrix only in the presence of a FBS gradient, demonstrating the active FBS-induced chemotaxis of metastatic cells. The mode of cell invasion in the presence of a chemoattractant was then studied. We observed most SUM-159 cells used mesenchymal-mode invasion, distinguished by elongated cell morphology with cell polarity (Figures 3b and S7). The initial cell morphology in the collagen gel was round, but after chemoattractant stimulation, cells formed protrusions at their leading edges and then acquired an elongated morphology toward the higher concentration of chemoattractant. Their trailing edges were then retracted to allow simultaneous forward movement (Figure S8). Some cells appeared to use an amoeboid invasion mode characterized by cell motility through plasma membrane blebbing.

Representative images of single SUM-159/GFP cells on the cell invasion array 96 h after the gradient generation are shown in Figure 3b,c. By comparing cell numbers from the top layer and the number of single-cell microwells after cell seeding (termed as fraction of invasive cells, Figure S9), the invasive capacity of a cancer cell can be evaluated. At any given time, the SUM-159 cells comprised a larger percentage of total cells in the top layer of the multiwell array than MCF-7 cells, demonstrating that SUM-159 cells have a higher invasion rate than MCF-7 cells (Figure 3d). For example, after 48 h, 18.5% of SUM-159 cells were located in the FBS-containing top layer of the microwells, but only 4.6% of MCF-7 cells had migrated toward the FBS. After 96 h, 34.2% of SUM-159 cells were located in the top layer, and only 8.1% of MCF-7 cells had migrated toward the FBS. We used confocal microscopy to image the full view of the cells and found most of the invasive cancer cells showed elongated cell morphology, and the noninvasive cells remaining on the bottom of the microwells exhibited round or cobblestone-like morphology.

Existing evidence suggests aberrant activation of a latent embryonic program, the epithelial-mesenchymal transition (EMT), as a central molecular event enhancing tumor cell invasion in response to environmental triggers.<sup>19</sup> Therefore, we investigated the invasiveness of cancer cells before and after EMT. MCF-7 cells transfected by the snail transcription factor or with empty vector were used in this assay. Cells transfected with Snail-6SA demonstrated loss of the epithelial markers E-cadherin and cytokeratin and gain of the mesenchymal marker vimentin.<sup>20</sup> However, MCF-7 cells with vector alone behaved as an epithelial cancer cell line, exhibiting cobblestone-like morphology. Comprehensive and statistical analyses showed few MCF-7 vector-only cells demonstrated chemotactic behavior, with only 8.4% of single MCF-7 vector-only cells located in the top layer of microwells after 96 h. Conversely, 26.2% of MCF-7 Snail-6SA cells moved toward the chemoattractant and arrived at the top layer of the microwells (Figure 3e). These results indicate that after EMT, single breast cancer cell invasive capacity was significantly enhanced. In addition to EMT, a subpopulation ( $\text{CD}44^+\text{CD}24^-$ ) of breast cancer cells exhibited enhanced invasive properties, an early step necessary for metastasis.<sup>21</sup> We used flow cytometry to isolate basal-like ( $\text{CD}44^+\text{CD}24^-$ ) and luminal-like ( $\text{CD}24^+\text{CD}44^-$ ) SUM-159 cells and then seeded them into the device to test their invasive capacity. As shown in Figure 3F, at any given time, a higher percentage of basal-like  $\text{CD}44^+$  SUM-159 cells, rather than luminal-like cells, occupies the top layers of the multiwell array.

**2.3. Invasion Assay at Different Cell Densities.** An invasion assay using a wide range of cell densities of SUM-159 and MCF-7 was performed using the gradient cell seeding method (Figures 2a and S10). After cell loading, bright-field and fluorescent images of cells located on the top layer of the microwells were recorded daily by adjusting the focal plane of the microscope (Figure 4a–d). The fraction of invasive cells in each microwell was calculated by counting cell numbers in the top layer of each microwell and dividing them by numbers of initial cells in the microwell; the average value at the same cell density was used to evaluate the invasive capacity of the cancer cell. For metastatic cancer cell line SUM-159, the fraction of invasive cells at a high cell density was greater than the fraction of invasive cells calculated at single-cell or low-cell density at all time points (Figure 4e). For example, after 96 h, 34% of single SUM-159 cells had migrated to the top layer of the microwells, and 46.5% of SUM-159 high-density cells had moved toward

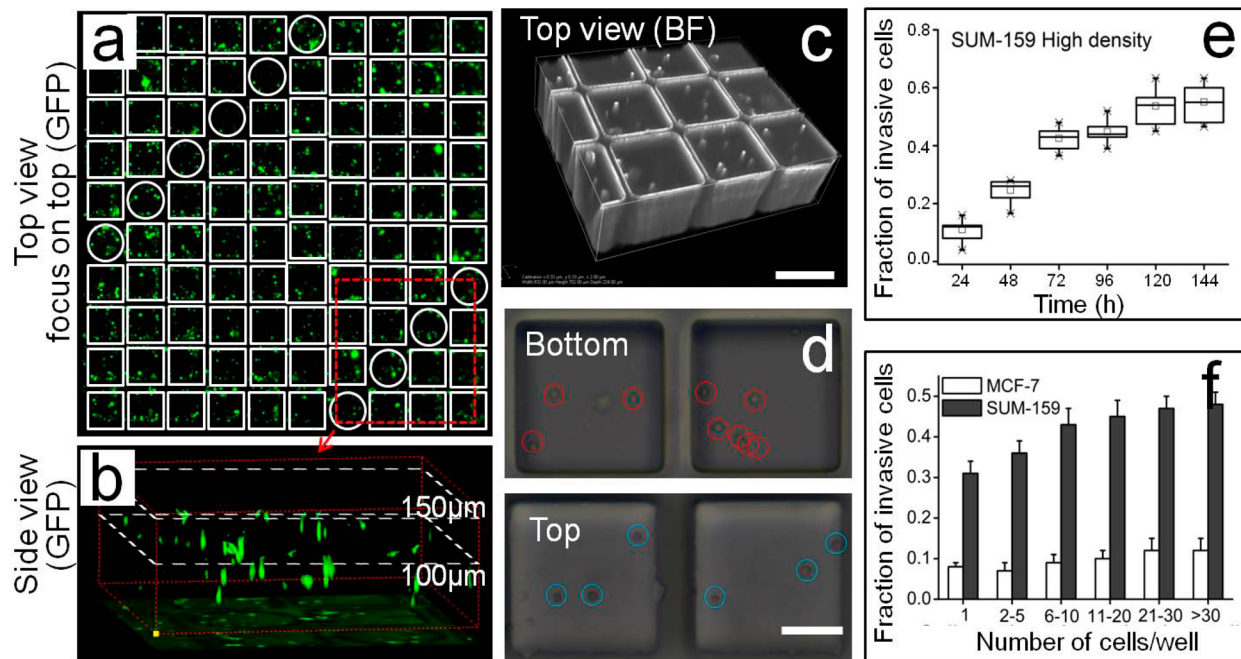


**Figure 4.** High-density cell invasion assay. (a) GFP image of invasive cells on the top layer of the microwells. (b) Image of a partial MI-Chip taken by a confocal microscope shows the cells located on the top layer of the microwells. (c) 3D bright-field (BF) image of invasive cells on the top layer of the microwells. Scale bar: 200  $\mu$ m. (d) Representative image taken by an optical microscope shows cells located on the top and bottom layers of the microwells (each circle represents a cell). Scale bar: 100  $\mu$ m (e). The fractions of invasive SUM-159 cells at a high-cell density (H) at different time points. (f) Comparison of fractions of invasive SUM-159 and MCF-7 cells at a gradient cell density after 96 h.

the FBS. As shown in Figure 4f, increased cell density enhanced the invasion capacity of the cancer cell. For the nonmetastatic MCF-7 cell line, increased cell density did not affect the fraction of invasive cells significantly. We also studied the impact of well shape to cell invasion by using two very different shapes shown in our original chip, round and square wells. For single or high-density cell invasion, our observed results showed very little difference between the two shapes, completely within the error range. Confocal microscopy was used to image the morphology of invading cancer cells at higher cell densities. In addition to the many cells already located in the top layer, additional cells had migrated more than 100  $\mu$ m. Most invasive cancer cells displayed elongated cell morphology. We suggest that the invading metastatic cells act in a cooperative manner using a form of autocrine and paracrine signaling, and increased cell density may contribute to tumor metastasis.<sup>7,22</sup>

Inhibition of cancer cell invasion should be based on two basic principles: to reduce the invasion (migration) velocity at the single-cell level and to disturb the cooperation between cancer cells and other cell types. In this study, we tested five small-molecule compounds that inhibit specific chemokines, growth factors, or kinases related to breast cancer metastasis on the MI-Chip (Table S1). Two modes of tumor cell movement are involved in invasion, proteolysis-guided mesenchymal movement and actomyosin-driven amoeboid movement. The inhibition of proteases, particularly MMPs, can convert the mode of migration from the former to the latter, and inhibition of Rho-associated kinase (ROCK) may convert the mode of migration from the latter to the former.<sup>23</sup> Therefore, we focused on MMPs and ROCK inhibitors.<sup>23,24</sup> The fractions of invasive cells treated with the five inhibitors are shown in Figure 5a.

We first studied MMP activities that contribute to potential cell invasiveness. MMP-1 specifically degrades type 1 collagen

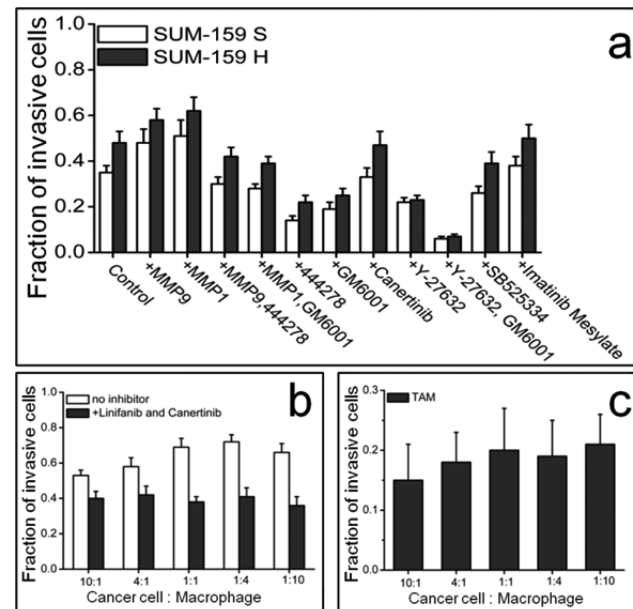


**Figure 5.** Effects of invasion inhibitors and macrophage cooperation on cancer cell migration. (a) Effects of small-molecule inhibitors on 3D cancer cell invasion at single-cell and high-cell densities. (b) Proportion of invasive MDA-MB-231 cells plated with TAMs at different ratios in the presence or absence of linifanib and canertinib. (c) Proportion of invasive TAM cells plated with MDA-MB-231 cells at different ratios. Error bars represent the standard deviation of replicates ( $n = 200$  microwells).

(used in our study), and MMP-9 cleaves type 1 collagen in its native form. MMP-1 (1  $\mu$ g/mL) and MMP-9 (0.5  $\mu$ g/mL) were included in the collagen gel, and the invasive capacity of SUM-159 cells at single-cell and high-cell densities was tested.

The presence of MMP-1 and MMP-9 increased the fraction of invasive cells at various cell densities. We then added the MMP inhibitors GM6001 and 444278 to the gel and found the invasive capacity of SUM-159 cells was reduced. In this situation, MMP inhibitors may block proteolysis-guided mesenchymal movement and cell invasion. The Rho-ROCK pathway is implicated in Ras-mediated transformation of tumor cells to display amoeboid movement in the 3D matrix, and we observed that treatment with a ROCK inhibitor (Y-27632) substantially attenuated invasiveness *in vitro* at both single-cell and high-cell densities. It is noteworthy that the fraction of invasive cells at a high cell density was similar to that observed in the single-cell assay, indicating ROCK inhibition reduces not only amoeboid movement but also cooperative interaction among cancer cells. The maximal level of inhibition was seen with Y-27632 and GM6001 together, in which proteolysis-guided mesenchymal movement and actomyosin-driven amoeboid movement were likely both inhibited. We also treated SUM-159 cells with canertinib (epithelial growth factor receptor inhibitor), SB525334 (transforming growth factor- $\beta$  inhibitor), and imatinib mesylate (platelet-derived growth factor receptor inhibitor), which all inhibited cell migration in a 2D assay in our lab.<sup>25</sup> These three inhibitors, however, did not significantly reduce the invasive capacity of SUM-159 cells in the 3D invasion device at either single-cell or high-cell density. Cells *in vivo* are situated within a complex 3D structure known as extracellular matrix. The shape and size of cells are affected by the physical and chemical environment of the extracellular matrix. Compared to 2D assays, our MI-Chip enables 3D capability and may provide more accurate cancer metastatic assays.

**2.4. Reverse Gradients to Study Cancer Cell and Macrophage Co-Invasion.** We next investigated whether directional movement of cancer cells in the presence of macrophages was associated with increased invasive behavior and if high TAM density corresponded to more vigorous cancer cell invasion. The metastatic MDA-MB-231 breast cancer cell line was used for this assay. The TAM cells were generated from monocyte-derived macrophages cultured in medium containing the supernatant of cancer cell culture medium with macrophage colony-stimulating factor (M-CSF, 100 ng/mL)<sup>26</sup> for the coinvasion assay. Stimulation with M-CSF and cancer cell culture medium led to a majority of elongated, fibroblast-like cells with enhanced adherence properties, whereas the absence of M-CSF and cancer cell culture medium resulted in a majority of round macrophages (Figure S11). Opposing gradients of the two types of cells (MDA-MB-231/GFP and TAM cells) on the same MI-Chip were generated by two consecutive sedimentation processes in opposite directions. After 96 h, the proportion of cells that migrated to the top layer was determined by viewing optical sections with a fluorescent microscope (Figure S12). When cultured alone, 38.2% of MDA-MB-231 cells invaded the top layer at 96 h, whereas in the presence of macrophages (10% of total cells), approximately 53% of MDA-MB-231 cells invaded the collagen and migrated to the top layer (Figures 5b and S13). An increased percentage of macrophages resulted in an increased proportion of MDA-MB-231 cells that migrated to the top layer; the peak value was approximately 72% when the ratio was 1:4 (cancer cells:macrophages). Further increases in macrophage numbers resulted in a reduction of cancer cell numbers and a reduction in the proportion of migrated cells. Even with decreased numbers, the proportion of migrating cancer cells was still

much higher than the proportion of cells at a low density in the absence of macrophages.

We also studied macrophage invasiveness by increasing their density in the MI-Chip and found no significant difference in migration (Figure 5C). Imposed gradients of epidermal growth factor (EGF) or colony-stimulating factor-1 (CSF-1) can induce invasion through an EGF/CSF-1 paracrine loop between cancer cells and macrophages.<sup>8b</sup> We treated the cells with linifanib (CSF-1R inhibitor) and canertinib (EGFR inhibitor) before seeding the device for the invasion assay. The results shown in Figure 5b indicate a disruption of this loop by blocking EGF and CSF-1 receptor signaling was sufficient to inhibit tumor cell migration and invasion. In clinical studies, macrophage density at the tumor site correlates with different stages of tumor growth.<sup>8a</sup> Our results show that, even at a low density, TAMs could promote invasion of breast carcinoma cells. These results suggest the prevention of cancer metastasis at an early stage may be achieved by inhibiting cooperation between macrophages and cancer cells.

### 3. DISCUSSION

The major cause of death in cancer patients with solid tumors is metastatic disease resulting from the shedding of tumor cells that subsequently migrate to anatomically distant sites. Tumor cell invasion is conventionally understood as the migration and invasion of individual cells or cell clusters that detach from the primary tumor.<sup>3,27</sup> However, cancer therapeutics targeting adhesion receptors or proteases to inhibit cell invasion and metastasis have yet to demonstrate effectiveness in clinical trials. Invasion mechanisms of cancer cells are still unclear, although cell reprogramming may be involved, allowing cells to maintain invasive properties via morphological and functional de-differentiation. For example, the mode of invasion may transition from mesenchymal movement to amoeboid movement. Therefore, the implementation of an effective assay to quantify and evaluate the invasive capacities of cancer cells may significantly aid in the development of novel cancer therapeutics.

In this study, we verified the capability of the MI-Chip for studying cancer metastasis by performing real-time 3D cell invasion assays using breast cancer cell lines at different cell densities. By calculating and analyzing fractions of invasive cells in each MI-Chip micowell, we quantified the invasive capacity of breast cancer cells, either alone or with tumor-associated macrophage cells over a wide range of cell densities that may correspond to different stages of malignancy. The small sample size (<1000 cells) used with the MI-Chip allows future analysis of the metastatic potential of primary or rare cells. By utilizing inhibitors of CSF-1 and EGF receptor signaling on two cell movement modes, we found that reducing the invasion (migration) velocity and blocking the partnership between cancer cells and immune cells may provide an effective method to reduce cell invasion and metastasis. The throughput can easily be extended to 80,000 or more, which is efficient to set up experiments in a high-throughput way. The cancer metastatic cascade involves cancer cells invading from primary tumor to circulating system, flowing within blood or lymph system, binding to second organ, and developing. Given such a complexity of the entire metastatic process, one device cannot fulfill all requirements. We focus on the 3D invasion assay to mimic the cells invading from primary tumor to blood vessels. This metastatic step is still relatively "static". In summary, this device provides a high-throughput platform for biologists and

clinicians to better perform assays that evaluate cancer cell behaviors related to metastasis.

## ■ ASSOCIATED CONTENT

### Supporting Information

Experimental details and additional information. This material is available free of charge via the Internet at <http://pubs.acs.org>.

## ■ AUTHOR INFORMATION

### Corresponding Authors

lqin@houstonmethodist.org

lzhou@houstonmethodist.org

### Notes

The authors declare no competing financial interest.

## ■ ACKNOWLEDGMENTS

We are grateful for Prof. Mien-Chie Hung's generous supply of MCF-7 and its derived cell lines. This study was funded by the Cancer Prevention and Research Institute of Texas (CPRIT-R1007), NIH-CA180083, Emily Herman Research Fund, and Golfers Against Cancer Foundation.

## ■ REFERENCES

- (1) Chaffer, C. L.; Weinberg, R. A. *Science* **2011**, *331*, 1559–64.
- (2) (a) Ridley, A. J.; Schwartz, M. A.; Burridge, K.; Firtel, R. A.; Ginsberg, M. H.; Borisy, G.; Parsons, J. T.; Horwitz, A. R. *Science* **2003**, *302*, 1704–9. (b) Joyce, J. A.; Pollard, J. W. *Nat. Rev. Cancer* **2009**, *9*, 239–52.
- (3) Friedl, P.; Alexander, S. *Cell* **2011**, *147*, 992–1009.
- (4) Hanahan, D.; Weinberg, R. A. *Cell* **2000**, *100*, 57–70.
- (5) Fidler, I. J. *Nat. Rev. Cancer* **2003**, *3*, 453–8.
- (6) (a) Chambers, A. F.; Groom, A. C.; MacDonald, I. C. *Nat. Rev. Cancer* **2002**, *2*, 563–72. (b) Sahai, E. *Nat. Rev. Cancer* **2007**, *7*, 737–49.
- (7) (a) Vedel, S.; Tay, S.; Johnston, D. M.; Bruus, H.; Quake, S. R. *Proc. Natl. Acad. Sci. U.S.A* **2013**, *110*, 129–34. (b) Rosen, P.; Misfeldt, D. S. *Proc. Natl. Acad. Sci. U.S.A* **1980**, *77*, 4760–3. (c) Roussos, E. T.; Condeelis, J. S.; Patsialou, A. *Nat. Rev. Cancer* **2011**, *11*, 573–87.
- (8) (a) Bingle, L.; Brown, N. J.; Lewis, C. E. *J. Pathol.* **2002**, *196*, 254–65. (b) Goswami, S.; Sahai, E.; Wyckoff, J. B.; Cammer, M.; Cox, D.; Pixley, F. J.; Stanley, E. R.; Segall, J. E.; Condeelis, J. S. *Cancer Res.* **2005**, *65*, 5278–83. (c) De Palma, M.; Lewis, C. E. *Cancer Cell* **2013**, *23*, 277–86.
- (9) Wu, J.; Wu, X.; Lin, F. *Lab Chip* **2013**, *13*, 2484–99.
- (10) Zaman, M. H.; Trapani, L. M.; Sieminski, A. L.; Mackellar, D.; Gong, H.; Kamm, R. D.; Wells, A.; Lauffenburger, D. A.; Matsudaira, P. *Proc. Natl. Acad. Sci. U.S.A* **2006**, *103*, 10889–94.
- (11) (a) Fraley, S. I.; Feng, Y.; Giri, A.; Longmore, G. D.; Wirtz, D. *Nat. Commun.* **2012**, *3*, 719. (b) Hofmann-Wellenhof, R.; Fink-Puches, R.; Smolle, J.; Helige, C.; Tritthart, H. A.; Kerl, H. *Melanoma Res.* **1995**, *5*, 311–9. (c) DiMilla, P. A.; Barbee, K.; Lauffenburger, D. A. *Biophys. J.* **1991**, *60*, 15–37. (d) Liu, L. Y.; Duclos, G.; Sun, B.; Lee, J.; Wu, A.; Kam, Y.; Sontag, E. D.; Stone, H. A.; Sturm, J. C.; Gatenby, R. A.; Austin, R. H. *Proc. Natl. Acad. Sci. U.S.A* **2013**, *110*, 1686–1691. (e) Lu, Y.; Chen, J. J.; Mu, L.; Xue, Q.; Wu, Y.; Wu, P. H.; Li, J.; Vortmeyer, A. O.; Miller-Jensen, K.; Wirtz, D.; Fan, R. *Anal. Chem.* **2013**, *85*, 2548–56.
- (12) Huang, Y.; Agrawal, B.; Sun, D.; Kuo, J. S.; Williams, J. C. *Biomicrofluidics* **2011**, *5*, 13412.
- (13) (a) Wu, M.; Swartz, M. *J. Biomech. Eng.* **2014**. (b) Song, Y.; Zhang, Y.; Bernard, P. E.; Reuben, J. M.; Ueno, N. T.; Arlinghaus, R. B.; Zu, Y.; Qin, L. *Nat. Commun.* **2012**, *3*, 1283.
- (14) (a) Xia, Y. N.; Whitesides, G. M. *Angew. Chem., Int. Ed.* **1998**, *37*, 551–575. (b) Xia, Y. N.; Whitesides, G. M. *Annu. Rev. Mater. Sci.* **1998**, *28*, 153–184. (c) Qin, D.; Xia, Y.; Whitesides, G. M. *Nat. Protoc.* **2010**, *5*, 491–502.
- (15) Yamanaka, Y. J.; Szeto, G. L.; Gierahn, T. M.; Forcier, T. L.; Benedict, K. F.; Brefo, M. S. N.; Lauffenburger, D. A.; Irvine, D. J.; Love, J. C. *Anal. Chem.* **2012**, *84*, 10531–10536.
- (16) Seubwai, W.; Kraiklang, R.; Wongkham, C.; Wongkham, S. *Asian Pac. J. Cancer Prev.* **2012**, *13*, 53–58.
- (17) Albini, A.; Iwamoto, Y.; Kleinman, H. K.; Martin, G. R.; Aaronson, S. A.; Kozlowski, J. M.; McEwan, R. N. *Cancer Res.* **1987**, *47*, 3239–3245.
- (18) Liu, W. Y.; Zhang, Y.; Thomopoulos, S.; Xia, Y. N. *Angew. Chem., Int. Ed.* **2013**, *52*, 429–432.
- (19) (a) Polyak, K.; Weinberg, R. A. *Nat. Rev. Cancer* **2009**, *9*, 265–273. (b) Thiery, J. P.; Acloque, H.; Huang, R. Y. J.; Nieto, M. A. *Cell* **2009**, *139*, 871–890.
- (20) Lien, H. C.; Hsiao, Y. H.; Lin, Y. S.; Yao, Y. T.; Juan, H. F.; Kuo, W. H.; Hung, M. C.; Chang, K. J.; Hsieh, F. J. *Oncogene* **2007**, *26*, 7859–7871.
- (21) Sheridan, C.; Kishimoto, H.; Fuchs, R. K.; Mehrotra, S.; Bhat-Nakshatri, P.; Turner, C. H.; Goulet, R.; Badve, S.; Nakshatri, H. *Breast Cancer Res.* **2006**, *8*, R59.
- (22) (a) Sung, S. Y.; Hsieh, C. L.; Wu, D.; Chung, L. W.; Johnstone, P. A. *Curr. Probl. Cancer* **2007**, *31*, 36–100. (b) Patsialou, A.; Wyckoff, J.; Wang, Y.; Goswami, S.; Stanley, E. R.; Condeelis, J. S. *Cancer Res.* **2009**, *69*, 9498–506.
- (23) Worthy lake, R. A.; Burridge, K. *J. Biol. Chem.* **2003**, *278*, 13578–13584.
- (24) Overall, C. M.; Lopez-Otin, C. *Nat. Rev. Cancer* **2002**, *2*, 657–672.
- (25) Zhang, Y.; Zhang, W.; Qin, L. *Angew. Chem., Int. Ed.* **2014**, *53*, 2344–2348.
- (26) Rey-Giraud, F.; Hafner, M.; Ries, C. H. *PLoS One* **2012**, *7*, e42656.
- (27) Friedl, P.; Wolf, K. *Nat. Rev. Cancer* **2003**, *3*, 362–74.